ENGINEERING RESEARCH JOURNAL (ERJ)
Vol. 1, No. 50 October 2021, pp.77-85
Journal Homepage: erj.bu.edu.eg

Experimental study and thermal performance evaluation of staggered cross flow heat exchangers of semi-circular tubes: II- Effect of attack angle

A.A.Alghrubah, M.A. Abd Elrahman, M.F. Abd Rabbo, Y.A. Al-Mashad, M.R. Salem

Mechanical Engineering Department, Faculty of Engineering at Shoubra, Benha University, Shoubra, Cairo, Egypt

Abstract : Bundles of tubes in cross flow are one of the frequently types of heat exchangers, which used in several applications. Therefore, enhancing their performance directly affects the working costs. In the present work, a pair of semicircular tubes (SCTs) is suggested to replace complete circular tube (CCT). Their performance attributes are examined for staggered tube bundle at several rates of airflow across the bundle and at several attack angles of their bases; from zero to 90°. It is reported that splitting the CCTs enhances the heat exchange rate as well growing the airflow resistance. Besides, increasing the base angle between 0° and 60° increases both the heat exchange and flow resistance. Their supreme increases are 105.1% and 47.4%, respectively, are obtained at 60° when compared with regular shape. While after 60° and below 90°, increasing the angle reduces these increases. The hydrothermal performance Indicator (*HTPI*) is presented to weigh the performance qualities. It is reported that *HTPI* is augmented by increasing the angle until 60° while it is constricted with increasing the angle after 60°.

Keywords: Staggered; Semi-circular tube; Base attack angle; Performance.

1. Introduction

The development of countries usually depends on several industries, which comprise heat exchange processes, whereas conversion, utilization, and recovery of the energy in every industrial, commercial, and domestic application include a heat exchange process. Flow across bundle of tubes is commonly applied in numerous applications [1-3]. The literature supplies very helpful studies on the thermal behaviour around tube bundles. Colburn [4] estimated a relationship to anticipate the heat load rate from staggered CCTs as a function of Re and Pr only. Other investigators [5-9] extended the work of Colburn on staggered/inline CCTs with another numbers of rows. Rabas et al. [10] experimentally analyzed the effect of fin density on the performance attributes of finned staggered CCT bank. The authors supplied correlations to predict the friction factor for finned CCT. Endres and Möller [11] experimentally analyzed the velocity and pressure oscillations of the crossflow in staggered/in-line CCT banks. Moawed [12] presented practical and numerically the thermal performance of airflow across single SCTs at constant heat flux settings. Khan et al. [13, 14] analyzed analytically the heating/cooling load rate from isothermal bundle of inline/staggered arrangements. In another study, Khan [15] proposed an analytical equation for isothermal staggered CCTs. Nada et al. [16] supplied experimental tests beside simulations for airflow across single SCT. The study was done for constant heat flux conditions and at different attack angles. The authors reported that the attack angle played a dramatic role in the heat exchange process. Jin et al. [17] simulated the heat exchange loading and pressure deterioration through H-type finned CCT bank. Amid the examined geometric parameters, CCT spacing has the furthermost vital effect. Chen et al. [18] performed practical tests to investigate the influence of incorporating H-type fins on the thermal performance attributes of CCT bank.

Lin et al. [19] numerically analyzed the flow and heat exchange through CCT bundle combined with grooved fins. The resulted maximum augmentation in the thermal performance was 27%. Wang et al. [20] practically compared the hydrothermal performance through CCT bundle equipped with three different kinds of vortex generators: plain, louver, and semi-dimple

Wang et al. [21] implemented experimental comparisons on the performance attributes of finned CCTs which are convoyed with vortex generators.

Jin et al. [22] simulated the flow outlines and heat exchange behaviour of airflow crossing an H-type finned CCTs. Song et al. [23] experimentally tested the heat load action of finned CCTs combined with curved delta winglet vortex generators. Ahmed et al. [24] numerically analyzed the laminar flow of water based nanofluid over isothermal staggered CCT bank. The effects of CCT spacings and nanoparticles loading were considered. Zhang et al. [25] studied the performance attributes of fractal rectangular/circular tube bank. In another study, Sahamifar et al. [26] recorded that the inlet Reynolds and Prandtl numbers did not affect the optimum dimensionless spacings in the turbulent regime. Huang et al. [27] simulated the thermal behaviour of a flow across inline and staggered CCT bank using lattice Boltzmann approach. Sakhaei et al. [28] practically and numerically analyzed the hydrothermal response of inclined tube bundle. Compared to flat bundle, it was recorded that the heat exchange rate and pressure loss were reduced by 30% and 60%, respectively. Lindqvist and Naess [29] considered numerically the flow actions across finned staggered CCTs. Lotfi and Sundén [30] simulated the flow patterns across plain finned staggered slotted elliptical tube bundle. It was observed that the proposed approach augmented the heat exchange by 15% rather than that of non-slotted case. From this survey, it is evident that a series of studies have been completed in practice / numerically to enhance the hydrothermal performance features of the tube banks. Several techniques have been suggested by researchers to achieve this. From the previous literature review, it is evident that no work has been tested by incorporating a pair of SCTs as a passive approach. The passive approaches were supplied by researchers to solve the problems incorporated with applying active ones, which require power source to do their missions [31-36]. The present work aims to test and evaluate the thermal performance of staggered pairs of SCT (Fig. 1). It is planned to consider seven attack angles of the bases of SCT and seven airflow rates.

Fig. 1 A snap of the SCTs.

2. Apparatus

The test rig conducted in the existing work includes two loops; heating air and cooling water cycles. The airflow loop comprises an open-loop stream, which includes a 5 hp suction-type blower, air valve controller, orifice plate meter, transition canal, pressure transducer, testing rig accompanied with the tubes, entry tunnel, straightener, and air heater. The cooling water loop comprises a closed-stream, which includes of a cooling unit, pump, valves, flow meter, entering/leaving headers, the tested tube bundle, and the connecting pipes. Fig. 2 supplies an outline of the air loop.

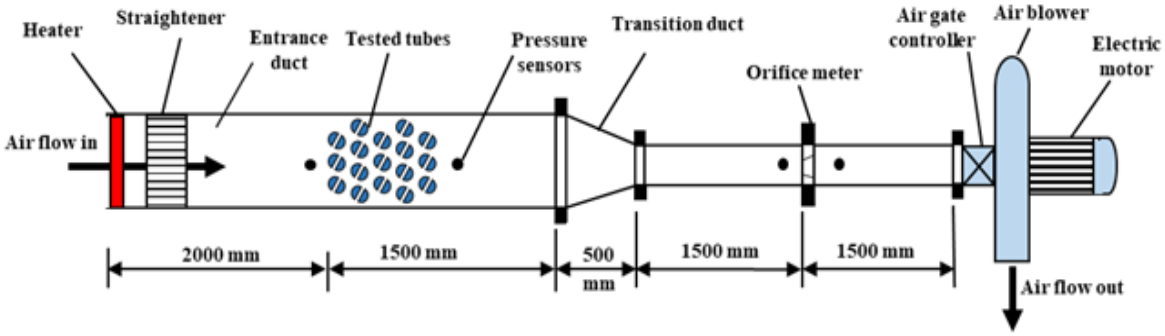

Fig. 2 A framework of the heating air path.

The incorporated heater has two stages, with 6 kW rating, and controlled via a pre-adjusted thermostat. The main rectangular flow path is fabricated of galvanized steel with dimensions of 950 mm width, 250 mm height and 3500 mm length. The exterior surface of the tunnel is enclosed with glass wool. Next the entrance section, the air then passes across the test rig, which is situated at 2000 mm from air entrance point. There are two apertures in the vertical sides of cross sections of 250 mm x 300 mm at which two headers are bolted. After departure the main duct, the air arrives the metering duct through the transition segment, which is formed as a converging unit with the aid of a metal former machine along with welding. The metering duct comprises two PVC pipes, are linked at the orifice plate, which is designed according to Miller [37]. The airflow rate is controlled via a damper.

The water-cooling system encompasses 100 litres insulated stainless steel reservoir, in which the heat is withdrawn via two cooling units of 20 kW capacity. A 3 hp power rating centrifugal pump with maximum capacity of 110 l/min is used to

circulate the cooling water. The water is pumped from the reservoir, flow meter, inlet header, circulated through the tubes, outlet header and is then backed to the reservoir. The tested tube bundles comprise 17 circular tubes or 34 semi-circular tubes; the number of rows in the flow direction is N_L = 5 while the numbers of tubes in the transverse direction are N_T = 3 and 4 in the odd and even rows, respectively. The tubes are organized as staggered

configuration. The geometry configurations are revealed in Fig. 3 and Table 1, in which the transversal (τ) and longitudinal (χ) spacing ratios, introduced to compare the space between the tubes in each direction compared with the tube outer diameter. The tubes are made of copper material of 14.45 and 15.88 mm internal and external diameters, respectively, of a total length of 1000 mm for each tube. To take shape of the SCTs, CCTs are longitudinally cut off via the plasma cutting instrument. Subsequently, a sheet of the same material, length, diameter, and thickness is longitudinally soldered.

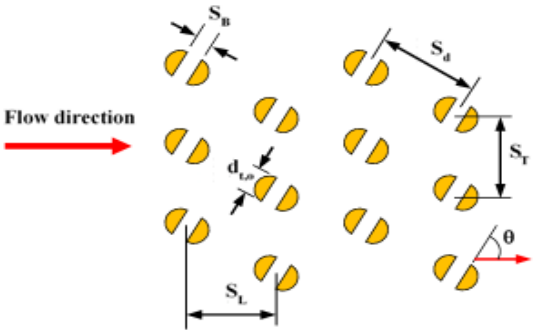

Fig. 4 Key dimensions of tested SCTs.

Table 1 Dimensions of the established tube banks.

No.	θ (°)	S_B (mm)	λ	S_T (mm)	τ	S_L (mm)	χ
Tube bank of CCTs							
1		———		31.75	2.0	31.75	2.0
Tube banks of SCTs							
2 to 8	0, 15, 30, 45, 60, 75, 90	6	0.378	31.75	2.0	31.75	2.0

Two galvanized steel cabinets are employed in the existing test rig to collect the water to/from the CCT/SCT bundle. The cabinets are of dimensions of 300x250x100 mm^3. One end of each header is bolted to a blind flange to block off these ends, while the other ends are bolted the duct. Wholly, sixteen housing dies are fabricated from 4 mm rectangular wooden sheets (320x270 mm^2, and 4 mm wall thickness) are set between the header and duct nipples. A laser cut machine is utilized to drill the dies, forming holes for the tubes of the tested tube bundles.Attention is considered to seal off any gap between the tubes and the holes in housing dies. The rate of airflow is assessed by assessing the pressure loss across the flow-orifice plate via a digital manometer (0.001–69 kPa pressure difference range, and accuracy of ±1 Pa). Water flow meter, 10–100 l/min range and accuracy of ±5% of reading is employed. Eight K-type thermocouples are employed to estimate the temperatures. Six junctions are inserted in the airstream; three at the entrance and another three at the exit of the test rig. Each three junctions are distanced from the upper surface of the duct by 16%, 32% and 50% of the duct height.

3. Experimental procedures

The onset of the tests begins by assembling the air blower, air gate regulator, orifice plate meter, transition channel, main duct, straightener, air electric heater, bundle of tubes, headers, cooling water system, piping, water flow meter, pump, thermocouples, and the digital manometer. Besides, the CCTs/SCTs are employed and settled in the duct according to the attributes in Table 1. The first step to gather the data from the testing system is to fill the cooling tank with water from the domestic water supply. Then, the blower, electric heater, the coolers, and the pump are switched on. The temperatures of both streams at test system inlets are regulated via the thermostats attached to the heater and cooler. The cooling water flow rate is regulated through the incorporated valves and rotameter, to permit flowing the designated flow rate in the primary line, while the overload fluid is backed to the reservoir. While the flow damper controls airflow rate through the test rig.During the tests, the steady attributes are presumed when a maximum alteration of 0.5°C is documented for 25 minutes by each thermocouple. The range of the operational settings is given in Table 2.

Table 2: Range of fluids functioning conditions.

Condition	Range or Value
Air-side	
Airflow rate, m³/s	0.285–1.677 ($2170 \le Re_{o,max} \le 12840$)
Inlet temperature, °C	50±1 ($Pr_o \approx 0.71$)
Water-side	
Total water flow rate, l/min	51.7 ($Re_i \approx 3320$)
Inlet temperature, °C	15 ($Pr_i \approx 7.95$)

4. Calculation equations and steps

In this study, the heat exchange is done as sensible heat which are determined using the inlet and outlet temperature besides the heat capacities of both fluids. Practically, an error is resulted between the two loads; max. deviation of 4.7% compared with the average

load of the heat exchanger. This load and $\Delta T_{L.M}$ are conducted to assess the $U_o A_{t,o}$. The factor F is calculated from Shah and Sekulić [38].

$$Q_o = \dot{m}_o Cp_o\left(T_{a,ave,i} - T_{a,ave,o}\right) \quad (1)$$

$$Q_i = \dot{m}_i Cp_i\left(T_{w,o} - T_{w,i}\right) \quad (2)$$

$$Q_{ave} = \frac{|Q_o| + |Q_i|}{2} \quad (3)$$

$$U_o A_{t,o} = \frac{Q_{ave}}{F \Delta T_{L.M}} \quad (4)$$

$$\Delta T_{L.M} = \frac{(\Delta T_i - \Delta T_o)}{ln\left[\frac{\Delta T_i}{\Delta T_o}\right]} = \frac{(T_{t,i} - T_{sh,o}) - (T_{t,o} - T_{sh,i})}{ln\left[\frac{T_{t,i} - T_{sh,o}}{T_{t,o} - T_{sh,i}}\right]} \quad (5)$$

The tube are thin and new, therefore other resistances are ignored, and now $U_o A_{t,o}$ is related only to convection resistances of the air and water. Because the water flow is fully developed and turbulent ($L_t/d_{t,h} > 10$), the $\overline{Nu}_i$ of the water is estimated using Gnielinski [39], Eq. (6), in which $Re_i = \left(4\dot{m}_{i,tube}\right)/\left(\pi d_{t,h} \mu_i\right)$, and f_i is assessed via Filonenko [40], through Eq. (7).

$$\overline{Nu}_i = \frac{\frac{f_i}{2}(Re_i - 1000)Pr_i}{1 + 12.7\sqrt{\frac{f_i}{2}}\left(Pr_i^{2/3} - 1\right)}\left[1 + \left(\frac{d_{t,h}}{L_t}\right)^{2/3}\right] \quad (6)$$

$$f_i = 0.25(1.82\, log\, Re_i - 1.64)^{-2} \quad (7)$$

Now, the $\overline{h}_i = \left(\overline{Nu}_i . k_i / d_{t,h}\right)$ is known. It should be noted that hydraulic diameter $d_{t,h}$ equals the tube inner diameter for CCTs, while $d_{t,h} = \left(\pi d_{t,i}/(\pi + 2)\right)$ in the case of SCTs. Besides, the surface area of the tubes is calculated as $17\pi d L_t$ for the circular tubes or $34 d L_t (0.5\pi + 1)$ for semicircular tubes. After that, the average convection coefficient and Nusselt number ($\overline{Nu}_o$) for the airside is obtained.

$$\frac{1}{U_i A_{t,o}} = \frac{1}{\overline{h}_o A_{t,o}} + \frac{1}{\overline{h}_i A_{t,i}} \quad (8)$$

$$\overline{h}_i = \frac{\overline{Nu}_i . k_i}{d_{t,h}} \quad (9)$$

$$\overline{Nu}_o = \frac{\overline{h}_o d_{t,o}}{k_o} \quad (10)$$

The air velocity measured in the empty main duct (u_o), is gotten from the calibrated orifice meter and continuity equation. While the maximum velocity ($u_{o,max}$) in the spaces between the tubes is calculated from Eq. (11), where $2S_d > (S_T + d_{t,o})$ [41]. The $u_{o,max}$ is incorporated to assess the air Reynolds and Stanton numbers besides the flow resistance [9];

$$u_{o,max} = \frac{u_o S_T}{S_T - d_{t,o}} \quad (11)$$

$$Re_{o,max} = \frac{u_{o,max} d_{t,o}}{\nu_o} \quad (12)$$

$$St_o = \frac{\overline{Nu}_o}{Re_{o,max} . Pr_o} \quad (13)$$

$$f_o = \frac{\Delta P_o}{2 N_L \rho_o u_{o,max}^2} \quad (14)$$

5. Validation

The validation of the procedures of assessing $\overline{Nu}_o$ and f_o is completed utilizing staggered CCT bundle. Colburn [4], Eq. (15) and Jakob [42], Eq. (16) are incorporated for this mission. Fig. 4 assures that their deviations do not differ by ±7.1% and ±6.1% for $\overline{Nu}_o$ and f_o, respectively.

$$\overline{Nu}_o = 0.33\, Re_{o,max}^{0.6} Pr_o^{1/3} \quad (15)$$

$$f_o = \left[0.25 + \frac{0.1175}{[(\tau - 1)^{1.08}]}\right] Re_{o,max}^{-0.16} \quad (16)$$

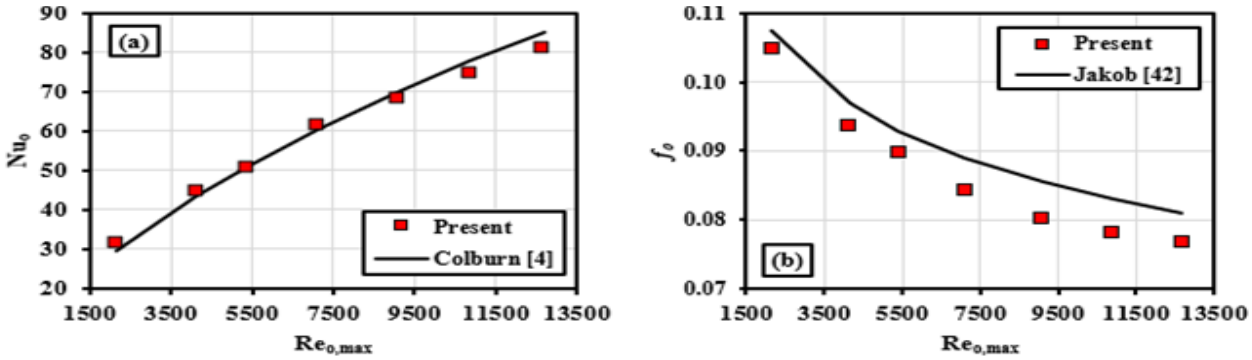

Fig. 4: Results of the validation tests; (a) $\overline{Nu}_o$, (b) f_o.

6. Results and discussions

6.1 Influence of base attack angle

In this analysis, seven angles of the base between zero and 90°are considered throughout the runs. The results are reported for staggered bundle of $\chi = \tau = 2.0$ and $\lambda = 0.378$. It is evidently shown that the direction of the base significantly influences the air hydrothermal characteristics. It is obvious that there are two different trends through two intervals of the attack angles. The experimental results assure that the incision of the tubes increase the $\overline{Nu}_o$ and f_o when compared with that of CCT bank, and their increases are grown up with expanding the angle in the extent of 0° to 60°, and these increases are then damped between angles 60° and 90°.Table 3 presents a summary of the effect of base angle compared with circular ones. It clear that their supreme increases are 105.1% and 47.4%, respectively, are obtained at 60°.

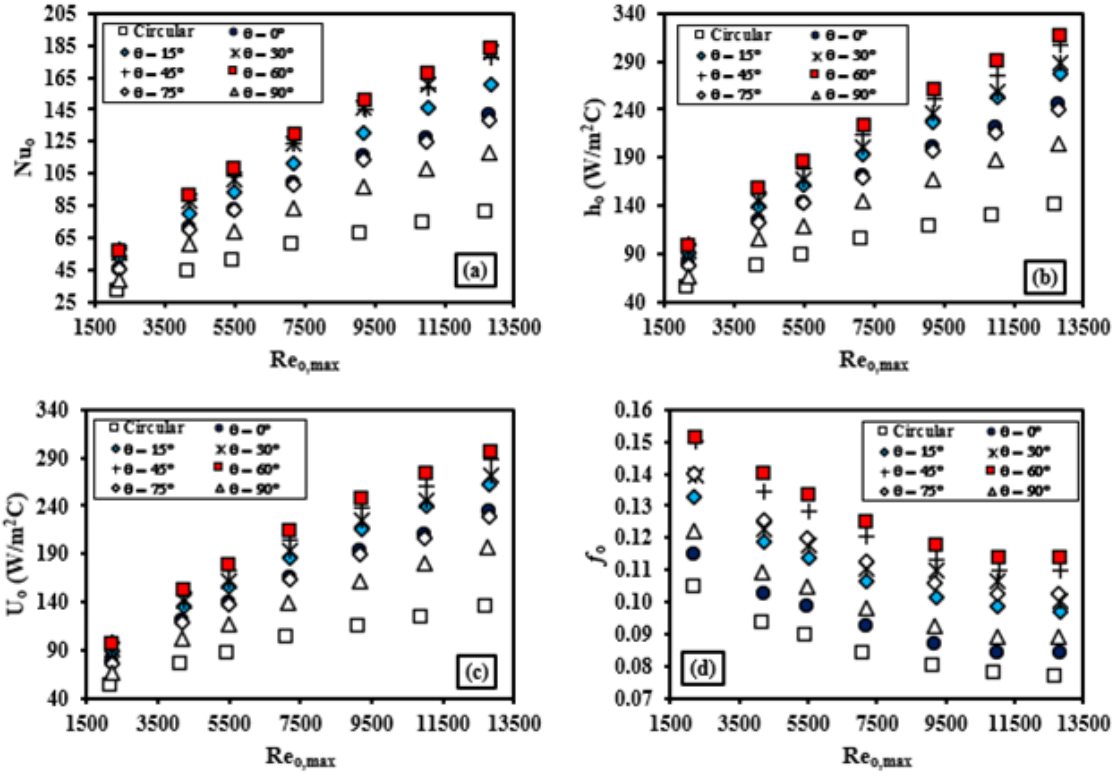

Fig. 5 Outputs of the performance parameters ($\tau = \chi = 2$, $\lambda = 0.378$); (a) $\overline{Nu}_o$, (b) $\overline{h}_o$, (c) U_o, (d) f_o.

Table 3: Effect of base angle compared with circular ones.

Specifications	θ = 0°	θ = 15°	θ = 30°	θ = 45°	θ = 60°	θ = 75°	θ = 90°
$\overline{Nu}_o$	58.5%	79.6%	86.1%	98.0%	105.1%	55.8%	33.0%
f_o	9.3%	26.5%	32.8%	42.6%	47.4%	33.2%	16.0%

Arranging the SCTs with 0° attack angle enlarges the surface area besides reducing the wake region at the rare of the tubes, which augments the cooling rate compared with the CCT case. Widening the angle more than 0°, forces the air stream coming from the distance formed between bases of the tubes to comminute with the mainstream, which strongly enhances the heat exchange and simultaneously increases the pressure decay. Furthermore, the reduction in the heat exchange coefficient and flow resistance with increasing the SCT angle from 60° and 90° can be attributed to the damping occurred for the flow velocity at the flow inlet between the two bases of each pair of the SCTs. This weakens the air flow velocity and reduces the mixing forces between the fluid layers, which consequently dampens the growths in the $\overline{Nu}_o$ and f_o.

6.2 Hydrothermal performance indicator

There are several expressions, which have been proposed to judge the feasibility of the incorporated enhancement technique. Here, the *HTPI* is judged via St_o and f_o[29], which are estimated when the SCTs and circular ones are engaged;

$$HTPI = \frac{St_{o,SCT}/St_{o,CCT}}{\left(f_{o,SCT}/f_{o,CCT}\right)^{1/3}} \quad (15)$$

The results state that the *HTPI* is increased by amplifying the angle of the SCTs from θ = 0° to θ = 60°, while it is then decreased with increasing the angle from θ = 60° to θ = 90°. As well, there is an augmentation by accelerating the flow. Moreover, the lowest and maximum values of *HTPI* are 1.15 and 2.01, got at θ = 90° and 60°, respectively.

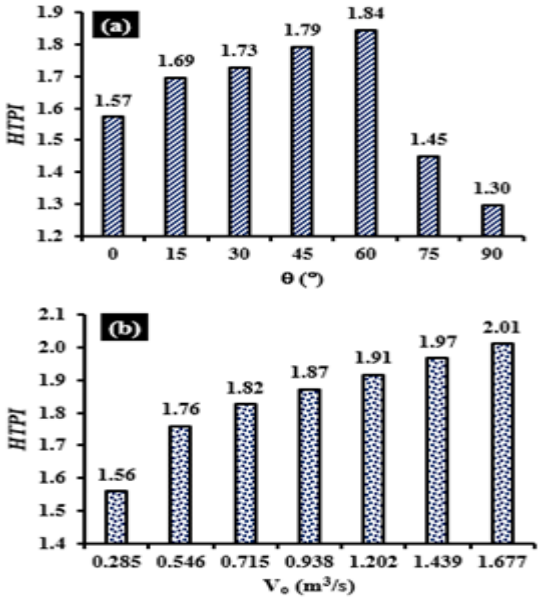

Fig. 6a,b: The average *HTPI;*(a) at different base directions, (b) at angle 60°, (c) at angle 90°.

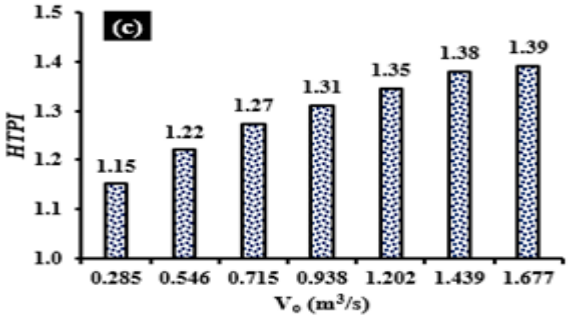

Fig. 6c: The average *HTPI;*(a) at different base directions, (b) at angle 60°, (c) at angle 90°.

7. Summary

This investigation introduces an experimental study on the hydrothermal attributes of staggered CCT or SCT bundles at several rates of airflow across the bundle. Throughout the tests, seven attack angles of the SCTs are examined. The outputs of this study state that:

- Splitting the tubes enhances the heat transfer rate as well growing the airflow pressure drop.
- The direction of the base of the SCT affects the hydrothermal performance with two different trends; in the range, 0°≤θ≤ 60°, the $\overline{Nu_o}$ and f_o are increased by mounting the attack angle. Compared with CCT, their maximum increases at θ = 60° are 105.1% and 47.4%, respectively. While in the range, 60°≤θ≤ 90°, the $\overline{Nu_o}$ and f_o are reduced with growing the attack angle.
- The *HTPI* is increased by increasing the attack angle in the range 0°≤θ≤ 60° and decreasing the attack angle in the range 60°≤θ≤ 90°.
- The maximum recorded value of *HTPI* is 2.01.

References

[1] M.R. Salem, "Experimental investigation on the hydrothermal attributes of MWCNT/water nanofluid in the shell-side of shell and semi-circular tubes heat exchanger", Applied Thermal Engineering, vol. 176, Article no. 115438, 2020.

[2] T.L. Bergman, A.S. Lavine, F.P. Incropera and D.P. Dewitt, "Fundamentals of Heat and Mass Transfer", 7th edition, John Wiley & Sons, 2011.

[3] M.R. Salem, K.M. Elshazly, R.Y. Sakr, R.K. Ali, Experimental study on convective heat transfer and pressure drop of water-based nanofluid inside shell and coil heat exchanger, PhD dissertation, Faculty of Engineering at Shoubra, Benha University, 2014.

[4] A.P. Colburn, "A method of correlating forced convection heat transfer data and a comparison with fluid friction", Transactions of the American Institute of Chemical Engineers, vol. 29, pp. 174-210, 1933.

[5] E.C. Huge, "Experimental investigation of effects of equipment size on convection heat transfer and flow resistance in cross flow of gases over tube banks", Transactions of ASME, vol. 59, pp. 573-581, 1937.

[6] O.P. Bergelin, E.S. Davis, H.L. Hull, "A study of three tube arrangements in unbaffled tubular heat exchangers", ASME Journal of Heat Transfer, vol. 71, pp. 369-374, 1949.

[7] O.P. Bergelin, G.A. Brown, S.C. Doberstein, "Heat transfer and fluid friction during flow across banks of tubes - IV: A study of the transition zone between viscous and turbulent flow", ASME Journal of Heat Transfer, vol. 74, pp. 953-959, 1952.

[8] A.J. Gram, C.O. Mackey, E.S. Monroe, "Convection heat transfer and pressure drop of air flowing across in-line tube banks: Part II - Correlation of data for ten-row-deep tube banks", Transactions of ASME, vol. 80, pp. 25-35, 1958.

[9] A. Zukauskas, "Heat transfer from tubes in cross flow", in J.P. Hartnett and T.F. Irvine, Jr., Eds., Advances in Heat Transfer, vol. 8, Academic Press, New York, 1972.

[10] T.J. Rabas, P.W. Eckels, R.A. Sabatino, "The effect of fin density on the heat transfer and pressure drop performance of low-finned tube banks", Chemical Engineering Communications, vol. 10(1-3), pp. 127-147, 1981.

[11] L.A. Endres, S.V. Möller, "On the fluctuating wall pressure field in tube banks", Nuclear Engineering and Design, vol. 203(1), pp. 13-26, 2001.

[12] M. Moawed, "Thermal performance of a cross flow heat exchanger with semi-circular tubes", ERJ Shoubra Faculty of Engineering, vol. 4, pp. 87-109, June 2005.

[13] W.A. Khan, J.R. Culham, M.M. Yovanovich, "Convection heat transfer from tube banks in crossflow: Analytical approach", International Journal of Heat and Mass Transfer, vol. 49 pp. 4831-4838, 2006.

[14] W.A. Khan, J.R. Culham, M.M. Yovanovich, "Analytical model for convection heat transfer from tube banks", Journal of Thermophysics and Heat Transfer, vol. 20(4), pp. 720-727, 2006.

[15] W.A. Khan, "Modeling of Fluid Flow and Heat Transfer for Optimization of Pin-Fin Heat Sinks", Ph.D. Thesis, University of Waterloo, Canada, 2004.

[16] S.A. Nada, H.El-Batsh, M. Moawed, "Heat transfer and fluid flow around semi-circular tube in cross flow at different orientations", Heat Mass Transfer, vol. 43, pp. 1157-1169, 2007.

[17] Y. Jin, G. Tang, Y. He, W. Tao, "Parametric study and field synergy principle analysis of H-type finned tube bank with 10 rows", International Journal of Heat and Mass Transfer, vol. 60, pp. 241-251, 2013.

[18] H. Chen, Y. Wang, Q. Zhao, H. Ma, Y. Li, Z. Chen, "Experimental investigation of heat transfer and pressure drop characteristics of H-type finned tube banks", Energies, vol. 7, pp. 7094-7104, 2014.

[19] Z. Lin, L. Wang, Y. Zhang, "Numerical study on heat transfer enhancement of circular tube bank fin heat exchanger with interrupted annular groove fin", Applied Thermal Engineering, vol. 73, 1465-1476, 2014.

[20] C. Wang, K. Chen, J. Liaw, C. Tseng, "An experimental study of the air-side performance of fin-and-tube heat exchangers having plain, louver, and semi-dimple vortex generator configuration", International Journal of Heat and Mass Transfer, vol. 80, pp. 281-287, 2015.

[21] C. Wang, K. Chen, J. Liaw, C. Tseng, "An experimental study of the air-side performance of fin-and-tube heat exchangers having plain, louver, and semi-dimple vortex generator configuration", International Journal of Heat and Mass Transfer, vol. 80, pp. 281–287, 2015.

[22] Y. Jin, Z. Yu, G. Tang, Y. He, W. Tao, "Parametric study and multiple correlations of an H-type finned tube bank in a fully developed region", Numerical Heat Transfer, Part A: Applications, vol. 70(1), pp. 64-78, 2016.

[23] K. Song, Z. Xi, M. Su, L. Wang, X. Wu, L. Wang, "Effect of geometric size of curved delta winglet vortex generators and tube pitch on heat transfer characteristics of fin-tube heat exchanger", Experimental Thermal and Fluid Science, vol. 82, pp. 8-18, 2017.

[24] M.A. Ahmed, M.M. Yaseen, M.Z. Yusoff, "Numerical study of convective heat transfer from tube bank in cross flow using nanofluid", Case Studies in Thermal Engineering, vol. 10, pp. 560-569, 2017.

[25] D. Zhang, Y. Shen, Z. Zhou, J. Qu, H. Xu, W. Cao, D. Song, F. Zhang, "Convection heat transfer performance of the fractal tube bank under cross flow", Fractals, vol. 26(5), article no. 1850073, 2018.

[26] S. Sahamifar, F. Kowsary, M.H. Mazlaghani, "Generalized optimization of cross-flow staggered tube banks using a subscale model", International Communications in Heat and Mass Transfer, vol. 105, pp. 46-57, 2019.

[27] J. Huang, C. Bao, Z. Jiang, X. Zhang, "A general approach of unit conversion system in lattice Boltzmann method and applications for convective heat transfer in tube banks", International Journal of Heat and Mass Transfer, vol. 135, pp. 873-884, 2019.

[28] M. Sakhaei, I.A. Abdi, F. Sabri, K. Hooman, "Experimental and numerical analysis of transient heat transfer from inclined tube bundles", Journal of Thermal Analysis and Calorimetry, vol. 140, pp. 1413-1426, 2020.

[29] K. Lindqvist, E. Naess, "On correction factors in thermal-hydraulic correlations for compact fin-tube bundles", Heat Mass Transfer, vol. 56, pp. 1713-1723, 2020.

[30] B. Lotfi, B. Sundén, "Development of new finned tube heat exchanger: Innovative tube-bank design and thermohydraulic performance", Heat Transfer Engineering, vol. 41(14), p.p.1209-1231, 2020.

[31] M.R. Salem, M.B. Eltoukhey, R.K. Ali, K.M. Elshazly, "Experimental investigation on the hydrothermal performance of a double-pipe heat exchanger using helical tape insert", International Journal of Thermal Sciences, vol. 124, pp. 496-507, 2018.

[32] K.M. Elshazly, R.Y. Sakr, R.K. Ali, M.R. Salem, "Effect of γ-Al_2O_3/Water Nanofluid on the Thermal Performance of Shell and Coil Heat Exchanger with Different Coil Torsions", Heat and Mass Transfer, vol. 53 (6), 1893-1903, 2017 .

[33] M.R. Salem, "Performance enhancement of a vapor compression refrigeration system using R134a/MWCNT-oil mixture and liquid-suction heat exchanger equipped with twisted tape turbulator", International Journal of Refrigeration, vol. 120, 357-369, 2020.

[34] S.M. Elshamy, M.T. Abdelghany, M.R. Salem, O.E. Abdellatif, "Based Al_2O_3 Nanofluid Including Diverse Coil Geometries: An Experimental Study", Journal of Nanofluids, vol. 9 (1), 13-23, 2020.

[35] M.R. Salem, H.A. El-Gammal, A.A. Abd-Elaziz, K.M. Elshazly, "Study of the performance of a vapor compression refrigeration system using conically coiled tube-in-tube evaporator and condenser", International Journal of Refrigeration, vol. 99, 393-407, 2019

[36] H.A. Refaey, E. Specht, M.R. Salem, "Influence of Fuel Distribution and Heat Transfer on Energy Consumption in Tunnel Kilns", International Journal of Advances in Engineering & Technology (IJAET), vol. 8(3), 281-293, 2015.

[37] R.W. Miller, "Flow measurement engineering handbook", 3rd edition, New York: McGraw-Hill, 2000.

[38] R.K. Shah, D.P. Sekulić, "Fundamentals of heat exchanger design", 6th edition, Hoboken, NJ: John Wiley & Sons, p. 189, 2003.

[39] V. Gnielinski, "New equations for heat and mass transfer in turbulent pipe and channel flow", International Chemical Engineering, vol. 16, pp. 359-368, 1976.

[40] G.K. Filonenko, "Hydraulic resistance of pipes (Hydraulischer Widerstand von Rohrleitungen)," Teploenergetika, vol. 1(4), pp. 40-44, 1954.

[41] F.W. Dittus, L.M.K. Boelter, "Heat transfer in automobile radiators of the tubular type", University of California Publications in Engineering, vol. 2, p. 433, 1930.

[42] M. Jakob, "Heat transfer and flow resistance in cross flow of gases over tube banks", Trans. ASME, vol. 60, p. 384, 1938.

Appendix A: Uncertainty Evaluation

For the CCT outer and inner diameters, spacing between the SCT-bases and pitches, the applied uncertainties are ±0.01 mm, while the uncertainty in the other measured dimensions is assumed to be ±0.5 mm. Thus, the extreme uncertainties related with the tube bundle geometry characteristics;

$$\frac{\omega_\lambda}{\lambda} = \pm\sqrt{\left(\frac{\omega_{S_B}}{S_B}\right)^2 + \left(\frac{-\omega_{d_{t,o}}}{d_{t,o}}\right)^2} = \pm\sqrt{\left(\frac{0.01}{2}\right)^2 + \left(\frac{-0.01}{15.88}\right)^2} = \pm 0.5\% \quad \textbf{(A1)}$$

$$\frac{\omega_\tau}{\tau} = \frac{\omega_\chi}{\chi} = \pm\sqrt{\left(\frac{\omega_{S_T}}{S_T}\right)^2 + \left(\frac{-\omega_{d_{t,o}}}{d_{t,o}}\right)^2} = \pm\sqrt{\left(\frac{0.01}{23.81}\right)^2 + \left(\frac{-0.01}{15.88}\right)^2} = \pm 0.08\% \quad \textbf{(A2)}$$

$$\omega_{S_T - d_{t,o}} = \pm\sqrt{\left(\omega_{S_T}\right)^2 + \left(-\omega_{d_{t,o}}\right)^2} = \pm\sqrt{(0.01)^2 + (-0..01)^2} = \pm 0.014 \text{ mm} \quad \textbf{(A3)}$$

$$\frac{\omega_{A_{t,o}}}{A_{t,o}} = \pm\sqrt{\left(\frac{\omega_{d_{t,o}}}{d_{t,o}}\right)^2 + \left(\frac{\omega_{L_t}}{L_t}\right)^2} = \pm\sqrt{\left(\frac{0.01}{15.88}\right)^2 + \left(\frac{0.5}{950}\right)^2} = \pm 0.08\% \quad \textbf{(A4)}$$

$$\frac{\omega_{A_{t,i}}}{A_{t,i}} = \pm\sqrt{\left(\frac{\omega_{d_{t,i}}}{d_{t,i}}\right)^2 + \left(\frac{\omega_{L_t}}{L_t}\right)^2} = \pm\sqrt{\left(\frac{0.01}{14.45}\right)^2 + \left(\frac{0.5}{950}\right)^2} = \pm 0.09\% \quad \textbf{(A5)}$$

$$\frac{\omega_{A_{bore}}}{A_{bore}} = \pm\sqrt{\left(\frac{\omega_W}{W}\right)^2 + \left(\frac{\omega_H}{H}\right)^2} = \pm\sqrt{\left(\frac{0.5}{250}\right)^2 + \left(\frac{0.5}{950}\right)^2} = \pm 0.21\% \quad \textbf{(A6)}$$

$$\frac{\omega_{A_{orifice}}}{A_{orifice}} = \pm\sqrt{\left(\frac{2\omega_{d_{orifice}}}{d_{orifice}}\right)^2} = \pm\left(\frac{2 * 0.5}{101.6}\right) = \pm 1\% \quad \textbf{(A7)}$$

In addition, the uncertainties in the temperature reading/difference estimations are;

$$\omega_{\Delta T_w} = \pm\sqrt{\left(\omega_{T_{w,o}}\right)^2 + \left(-\omega_{T_{w,i}}\right)^2} = \pm 0.5 * \sqrt{2} = \pm 0.71℃ \quad \textbf{(A8)}$$

$$\omega_{\Delta T_a} = \pm\sqrt{\left(\frac{\partial \Delta T_a}{\partial T_{a,i}}\omega_{T_{a,i}}\right)^2 + \left(\frac{\partial \Delta T_a}{\partial T_{a,o}}\omega_{T_{a,o}}\right)^2} = \pm 0.04 * \sqrt{2} = \pm 0.06℃ \quad \textbf{(A9)}$$

$$\omega_{\Delta T_i} = \omega_{\Delta T_o} = \pm\sqrt{\left(\frac{\partial \Delta T_i}{\partial T_{a,ave,i}}\omega_{T_{a,ave,i}}\right)^2 + \left(\frac{\partial \Delta T_i}{\partial T_{w,o}}\omega_{T_{w,o}}\right)^2} = \pm\sqrt{(0.04)^2 + (0.5)^2} \cong \pm 0.5℃ \quad \textbf{(A10)}$$

$$\omega_{\Delta T_{L.M}} = \pm\frac{\omega_T\sqrt{2}}{\ln\left[\frac{\Delta T_i}{\Delta T_o}\right]}\sqrt{2 - 2\Delta T_{L.M}\left(\frac{1}{\Delta T_i} + \frac{1}{\Delta T_o}\right) + \Delta T_{L.M}^2\left(\frac{1}{\Delta T_i^2} + \frac{1}{\Delta T_o^2}\right)} \quad \textbf{(A11)}$$

The uncertainty in the water volume flow rate is ±1.67%. Then the uncertainties in other water flow characteristics are;

$$\frac{\omega_{\dot m_w}}{\dot m_w} = \pm\sqrt{\left(\frac{\omega_{\rho_w}}{\rho_w}\right)^2 + \left(\frac{\omega_{\dot V_w}}{\dot V_w}\right)^2} = \pm\sqrt{(0.001)^2 + (0.0167)^2} = \pm 1.67\% \quad \textbf{(A12)}$$

$$\frac{\omega_{Re_i}}{Re_i} = \pm\sqrt{\left(\frac{\omega_{\dot m_w}}{\dot m_w}\right)^2 + \left(\frac{\omega_{d_{t,h}}}{d_{t,h}}\right)^2 + \left(\frac{\omega_{\mu_i}}{\mu_i}\right)^2} \cong \pm 1.67\% \quad \textbf{(A13)}$$

Moreover, the extreme uncertainties in the airflow characteristics are;

$$\frac{\omega_{u_o}}{u_o} = \pm\sqrt{\left(\frac{0.7566\ \omega_{\Delta H_o}}{\Delta H_o}\right)^2 + \left(\frac{\omega_{A_{bore}}}{A_{bore}}\right)^2 + \left(\frac{\omega_{A_{orifice}}}{A_{orifice}}\right)^2} \cong \pm 4.29\% \quad \textbf{(A14)}$$

$$\frac{\omega_{u_{o,max}}}{u_{o,max}} = \pm\sqrt{\left(\frac{\omega_{u_o}}{u_o}\right)^2 + \left(\frac{\omega_{S_T}}{S_T}\right)^2 + \left(\frac{\omega_{S_T - d_{t,o}}}{S_T - d_{t,o}}\right)^2} \cong \pm 4.29\% \quad \textbf{(A14)}$$

$$\frac{\omega_{Re_{o,max}}}{Re_{o,max}} = \pm\sqrt{\left(\frac{\omega_{u_{o,max}}}{u_{o,max}}\right)^2 + \left(\frac{\omega_{d_{t,o}}}{d_{t,o}}\right)^2 + \left(\frac{\omega_{\nu_o}}{\nu_o}\right)^2} \cong \pm 4.29\% \quad \textbf{(A15)}$$

$$\frac{\omega_{\dot V_o}}{\dot V_o} = \pm\frac{0.7566\ \omega_{\Delta H_{orifice}}}{\omega_{\Delta H_{orifice}}} = \pm 0.32\%\ (\text{max. value}) \quad \textbf{(A16)}$$

$$\frac{\omega_{\dot m_o}}{\dot m_o} = \pm\sqrt{\left(\frac{\omega_{\dot V_o}}{\dot V_o}\right)^2 + \left(\frac{\omega_{\rho_o}}{\rho_o}\right)^2} = \pm 0.33\%\ (\text{max. value}) \quad \textbf{(A17)}$$

Now, the extreme uncertainties in the hydrothermal performance attributes are:

$$\frac{\omega_{Q_o}}{Q_o} = \pm\sqrt{\left(\frac{\omega_{\dot{m}_o}}{\dot{m}_o}\right)^2 + \left(\frac{\omega_{Cp_o}}{Cp_o}\right)^2 + \left(\frac{\omega_{\Delta T_a}}{\Delta T_a}\right)^2} = \pm 4\% \quad \textbf{(A18)}$$

$$\frac{\omega_{Q_i}}{Q_i} = \pm\sqrt{\left(\frac{\omega_{\dot{m}_i}}{\dot{m}_i}\right)^2 + \left(\frac{\omega_{Cp_i}}{Cp_i}\right)^2 + \left(\frac{\omega_{\Delta T_w}}{\Delta T_w}\right)^2} = \pm 1.7\% \quad \textbf{(A19)}$$

$$\omega_{Q_{ave}} = \pm\frac{1}{2}\sqrt{(\omega_{Q_o})^2 + (\omega_{Q_i})^2} = \pm 2.19\% \quad \textbf{(A20)}$$

$$\frac{\omega_{U_o}}{U_o} = \pm\sqrt{\left(\frac{\omega_{Q_{ave}}}{Q_{ave}}\right)^2 + \left(\frac{-\omega_{A_{t,o}}}{A_{t,o}}\right)^2 + \left(\frac{-\omega_{\Delta T_{L.M}}}{\Delta T_{L.M}}\right)^2} = \pm 2.3\% \quad \textbf{(A21)}$$

$$\frac{\omega_{\overline{Nu}_i}}{\overline{Nu}_i} = \pm\sqrt{\left(\frac{0.8\,\omega_{Re_i}}{Re_i}\right)^2 + \left(\frac{0.4\,\omega_{Pr_i}}{Pr_i}\right)^2} \cong \pm 1.3\% \quad \textbf{(A22)}$$

$$\frac{\omega_{\overline{h}_i}}{\overline{h}_i} = \pm\sqrt{\left(\frac{\omega_{\overline{Nu}_i}}{\overline{Nu}_i}\right)^2 + \left(\frac{\omega_{k_i}}{k_i}\right)^2 + \left(\frac{-\omega_{d_{t,h}}}{d_{t,h}}\right)^2} \cong \pm 1.4\% \quad \textbf{(A23)}$$

$$\omega_{\overline{h}_o} = \pm\sqrt{\left(\frac{\partial\overline{h}_o}{\partial U_o}\omega_{U_o}\right)^2 + \left(\frac{\partial\overline{h}_o}{\partial A_{t,o}}\omega_{A_{t,o}}\right)^2 + \left(\frac{\partial\overline{h}_o}{\partial A_{t,i}}\omega_{A_{t,i}}\right)^2 + \left(\frac{\partial\overline{h}_o}{\partial\overline{h}_i}\omega_{\overline{h}_i}\right)^2} \cong \pm 4.7\% \quad \textbf{(A24)}$$

$$\frac{\omega_{\overline{Nu}_o}}{\overline{Nu}_o} = \pm\sqrt{\left(\frac{\omega_{\overline{h}_o}}{\overline{h}_o}\right)^2 + \left(\frac{\omega_{d_{t,o}}}{d_{t,o}}\right)^2 + \left(\frac{-\omega_{k_o}}{k_o}\right)^2} \cong \pm 4.7\% \quad \textbf{(A25)}$$

$$\frac{\omega_{\overline{Nu}_o}}{\overline{Nu}_o} = \pm\sqrt{\left(\frac{\omega_{\overline{h}_o}}{\overline{h}_o}\right)^2 + \left(\frac{\omega_{d_{t,o}}}{d_{t,o}}\right)^2 + \left(\frac{-\omega_{k_o}}{k_o}\right)^2} \cong \pm 4.7\% \quad \textbf{(A26)}$$

$$\frac{\omega_{St_o}}{St_o} = \pm\sqrt{\left(\frac{\omega_{\overline{Nu}_o}}{\overline{Nu}_o}\right)^2 + \left(\frac{\omega_{Re_{o,max}}}{Re_{o,max}}\right)^2 + \left(\frac{-\omega_{Pr_o}}{Pr_o}\right)^2} \cong \pm 6.3\% \quad \textbf{(A27)}$$

$$\frac{\omega_{f_o}}{f_o} = \pm\sqrt{\left(\frac{\omega_{\Delta P_o}}{\Delta P_o}\right)^2 + \left(\frac{\omega_{\rho_o}}{\rho_o}\right)^2 + \left(\frac{-2\omega_{u_{o,max}}}{u_{o,max}}\right)^2} \cong \pm 5.8\% \quad \textbf{(A28)}$$

$$\frac{\omega_{HTPI}}{HTPI} = \pm\sqrt{\left(\frac{\omega_{St_{o,SCT}}}{St_{o,SCT}}\right)^2 + \left(\frac{\omega_{St_{o,CCT}}}{St_{o,CCT}}\right)^2 + \left(\frac{\frac{1}{3}\omega_{f_{o,SCT}}}{f_{o,SCT}}\right)^2 + \left(\frac{\frac{1}{3}\omega_{f_{o,CCT}}}{f_{o,CCT}}\right)^2} \cong \pm 6.7\% \quad \textbf{(A29)}$$

Nomenclatures

A	Area, m^2
Cp	Specific heat, $J/kg\,.\,℃$
d	Diameter, m
f	Fanning friction factor
h	Convection heat transfer coefficient, $W/m^2\,.\,℃$
k	Thermal conductivity, $W/m\,.\,℃$
L	Length, m
$\dot{m}$	Mass flow rate, kg/s
P	Pressure, Pa
Q	Heat transfer rate, W
S	Spacing between the bases of a pair of SCTs, m
T	Temperature, ℃ or K
u	Velocity, m/s
$\dot{V}$	Volume flow rate, m^3/s

Dimensionless groups

$\overline{Nu}$	Average Nusselt number
Pr	Prandtl number
Re	Reynolds number
St	Stanton number

Greek letters

Δ	Differential
π	Constant ≅ 3.1416
λ	Base gap ratio
μ	Dynamic viscosity, $kg/m\,.\,s$
ρ	Density, kg/m^3
θ	Attack angle, °

Superscripts and subscripts

ave	Average
B	Base
cir	Circular
h	Hydraulic
i	Inner or inlet or internal
LM	Logarithmic Mean
m	Mean
max	Maximum
o	Out or outer
s	Surface
t	Tube
V	Vertical

Acronyms and abbreviations

CCT	Complete Circular Tube
HTPI	Hydrothermal Performance Indicator
SCT	Semi-Circular Tube